CHAPTER 3

A Planar Shaped-Beam Antenna with dielectric grating

In the previous chapter, a planar shaped-beam antenna using metal grating was fabricated, and its radiation patterns at various different operation frequencies were measured. The good agreement between the measured and calculated results was obtained. Besides, the numerical simulation for inspecting the parameters affecting the radiation pattern were also carried out. In this chapter, another planar shaped-beam antenna with dielectric grating instead of metal grating was designed. Besides, a computer program was developed to calculate the field distribution in the structure and the far-field radiation pattern. We not only demonstrated the calculated radiation pattern, but also numerically discussed the variation of the radiation pattern against the changes in the following parameters (sensitivity analysis), such as the relative dielectric constant, thickness of the dielectric grating layer, and the location of the excitation source. Moreover, since the structure is closed in the backward and sideward directions, their radiation is inconsiderable in those directions. We only demonstrated the forward radiation pattern for in numerical examples.

3.1. STRUCTURE CONFIGURATION

As shown in figure 14, the antenna under consideration contains an air separator with thickness denoted as d_1, sandwiched between a metal plate and dielectric rods array (dielectric grating) filled in a parallel-plate waveguide. The width, length and thickness of each dielectric rod are a, l and tg, respectively. The period of the dielectric rod array is b. The structure is excited by a line source made up of a monopole. The distance from the line source to the metal plate is d_2. The width of the antenna is $(N\text{-}1)b+a+2d_a$, where N is the number of dielectric rods along the x direction. To have a symmetric radiation pattern in the forward direction, the line

source is placed at the center along the x direction.

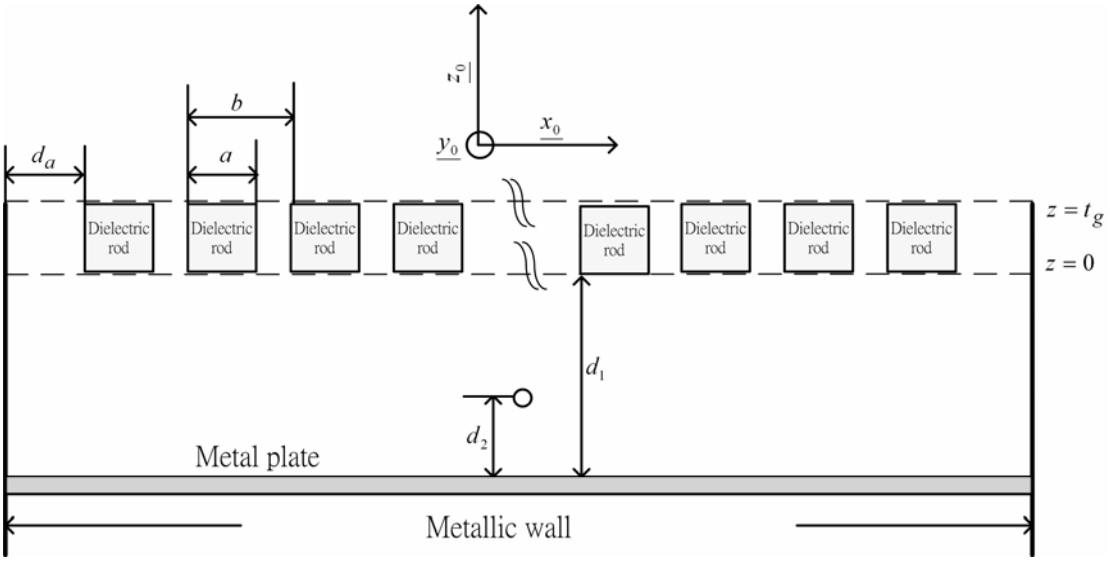

Figure 14: The structure configuration and parameters assignment of the shaped-beam antenna

3.2. METHOD OF ANALYSIS

For the theoretical formulation, since the length of the structure along the *y*-direction is greater than five times of the operation wavelength, the structure is assumed to have no electromagnetic fields variation along the *y* the direction. Accordingly, the electromagnetic field problem could be regarded as a two-dimensionally boundary-value problem. The individual polarization (E_y mode) is considered only, without dealing with the cross-polarization problem. Returning to figure 14, since the structure has only one open end along the +*z* direction, the radiation far-field can be approximately calculated by the equivalent sources, including the electric- and magnetic- source, induced on the outmost surface of the dielectric grating. To obtain the electromagnetic fields on the outer surface of dielectric grating, we have to solve the electromagnetic fields in the dielectric grating consisting of dielectric rods. Because the eigen-functions on the cross-section direction in the grating region can be determined, the mode-matching method was employed to formulate the electromagnetic boundary-value problem. By matching the tangential electric and magnetic fields across the discontinuities between the dielectric grating and the PPWG, the original electromagnetic fields problem can be converted into the cascades of transmission line networks including an excitation current source. Therefore, the modal voltage and current everywhere are determined by solving the transmission-line network.

The electric and magnetic fields in the PPWG can be expressed in terms of the superposition of PPWG modes, which are given below.

$$\overline{E}_y(x,z) = -\sum_{n=1}^{\infty} \overline{V}_n(z)\overline{\phi}_n(x) \qquad (3.1)$$

$$\overline{H}_x(x,z) = \sum_{n=1}^{\infty} \overline{I}_n(z)\overline{\phi}_n(x) \qquad (3.2)$$

with $$\bar{\phi}_n(x) = \sqrt{\frac{2}{w}} \sin\left(\frac{n\pi x}{w}\right) \tag{3.3}$$

where the $\bar{V}$'s and $\bar{I}$'s denote the voltage and current waves in each parallel-plate waveguide, which satisfy the transmission line equations along the *z* direction given as follow

$$\frac{d\bar{V}_n(z)}{dz} = -j\bar{k}_{zn}\bar{Z}_n\bar{I}_n(z) \tag{3.4}$$

$$\frac{d\bar{I}_n(z)}{dz} = -j\bar{k}_{zn}\bar{Y}_n\bar{V}_n(z) \tag{3.5}$$

where the $\bar{k}_{zn}$ and $\bar{Z}_n$ ($\bar{Y}_n$) are the propagation constant and impedance (admittance) along the *z*-direction, which are written as

$$\bar{k}_{zn} = \sqrt{k_0\varepsilon_a - \left(\frac{n\pi}{w}\right)^2} \tag{3.6}$$

$$\bar{Z}_n = \omega\mu_o / \bar{k}_{zn} \tag{3.7}$$

The mode function and the propagation wave number of dielectric grating filled in PPWG is determined utilizing the transverse resonance technique, and the electric and magnetic fields in the dielectric grating can be expressed in terms of the superposition of these modes, which are given below.

$$E_y(x,z) = -\sum_{n=1}^{\infty} V_n(z)\phi_n(x) \tag{3.8}$$

$$H_x(x,z) = \sum_{n=1}^{\infty} I_n(z)\phi_n(x) \tag{3.9}$$

Based on the electromagnetic boundary conditions, the tangential electric and magnetic field must be continuous the discontinuities between the dielectric grating and the PPWG, $z = t_g$ and $z = 0$ as shown in figure 10.

This yields the following equations:

$$\sum_{n=1}^{\infty} \bar{V}_n\left(t_g^+\right)\bar{\phi}_n(x) = \sum_{n=1}^{\infty} V_n\left(t_g^-\right)\phi_n(x) \tag{3.10}$$

$$\sum_{n=1}^{\infty} \bar{I}_n\left(t_g^+\right)\bar{\phi}_n(x) = \sum_{n=1}^{\infty} I_n\left(t_g^-\right)\phi_n(x) \tag{3.11}$$

We can determine the relationships for the voltage and current on both sides of the interface by taking the scalar products on both sides of the two equalities above with the mode function of PPWG or dielectric grating. In the matrix form, they are given by

$$\bar{\mathbf{V}}\left(t_g^+\right) = \mathbf{P}\mathbf{V}\left(t_g^-\right) \tag{3.12}$$

$$\bar{\mathbf{P}}\bar{\mathbf{V}}\left(t_g^+\right) = \mathbf{V}\left(t_g^-\right) \tag{3.13}$$

$$\bar{\mathbf{I}}\left(t_g^+\right) = \mathbf{P}\mathbf{I}\left(t_g^-\right) \tag{3.14}$$

$$\mathbf{P} = \{P_{mn}\} \tag{3.15}$$

$$P_{mn} = \left\langle \phi_m(x) \middle| \bar{\phi}_n(x) \right\rangle \tag{3.16}$$

where **V**'s and **I** 's are the column vectors with V_n and I_n as their element at the n-th entries. **P** is the coupling matrix with its elements P_{mn} representing the electromagnetic field coupling coefficient between m-th mode in dielectric grating region and n-th mode in PPWG region. In addition, $\bar{\mathbf{P}}$ represents the transpose of matrix **P**. After obtaining the coupling matrix between PPWG and grating region, we could check the numerical accuracy of the matrix. If the matrix is not accurate enough, the power will not be conserved and the electromagnetic field will not be continuous at the interface. Substituting (3.13) into (3.12), we have the unitary condition:

$$\mathbf{P}\bar{\mathbf{P}} = \mathbf{I} \tag{3.17}$$

Where **I** is the identity matrix. Equation (3.17) may be utilized to check that

whether the coupling matrix is accurate or not in numerical computing.

Having the relationship between the voltage and current wave in PPWG region and dielectric grating at the junction discontinuous, we can develop the input-output relation of a dielectric grating layer, including the input impedance matrix and the voltage transfer matrix. Firstly, if the output admittance of the dielectric grating layer is given by

$$\bar{\mathbf{I}}\left(t_g^+\right) = \overline{\mathbf{Y}}_l \overline{\mathbf{V}}\left(t_g^+\right) \tag{3.18}$$

where t_g^+ represents the output surface position of the dielectric grating, in the PPWG region. Substituting (18) into equations (12), (13) and (14), we could obtain the output admittance matrix at $z = t_g^-$, which is given below.

$$\mathbf{I}\left(t_g^-\right) = \mathbf{Y}_l \mathbf{V}\left(t_g^-\right) \tag{3.19}$$

with $\mathbf{Y}_l = \overline{\mathbf{P}}\overline{\mathbf{Y}}_l \mathbf{P}$ (3.20)

When the input admittance matrix is determined, we could derive the input impedance matrix at $z = 0^+$, which is defined in the dielectric grating region, given as

$$\mathbf{\Gamma}\left(t_g^-\right) = \left(\mathbf{Y} + \mathbf{Y}_l\right)^{-1}\left(\mathbf{Y} - \mathbf{Y}_l\right) \tag{3.21}$$

$$\mathbf{\Gamma}\left(0^+\right) = \exp(-j\mathbf{k}_z t_g)\mathbf{\Gamma}\left(t_g^-\right)\exp(-j\mathbf{k}_z t_g) \tag{3.22}$$

$$\mathbf{Z}_{in}\left(0^+\right) = \left(\mathbf{1} + \mathbf{\Gamma}\left(0^+\right)\right)\left(\mathbf{1} - \mathbf{\Gamma}\left(0^+\right)\right)^{-1}\mathbf{Z} \tag{3.23}$$

$$\mathbf{T}\left(t_g^+ \to 0^+\right) = \left(1 + \mathbf{\Gamma}\left(t_g^-\right)\right)\exp(-j\mathbf{k}_z t_g)\left(1 + \mathbf{\Gamma}\left(0^+\right)\right)^{-1} \tag{3.24}$$

where Y is the characteristic admittance matrix along the z-direction in the dielectric grating layer. The parameter $\mathbf{k}_z$ is a diagonal matrix with each element representing the z-direction propagation constant of each mode in the dielectric grating layer. The matrix T defines the relationship for the voltage waves at the input and output

interface of the dielectric grating layer which is given below

$$\mathbf{V}\left(t_g^+\right)=\mathbf{T}\left(t_g^+\to 0^+\right)\mathbf{V}\left(0^+\right) \tag{3.25}$$

Moreover, the input impedance matrix, defined at the input interface in the air separator layer, and the voltage transfer matrix, defining the relationship between the output and input voltage waves through the dielectric grating layer, is given below

$$\mathbf{Z}_{in}\left(0^-\right)=\mathbf{P}\mathbf{Z}_{in}\left(0^-\right)\mathbf{P} \tag{3.26}$$

$$\overline{\mathbf{T}}\left(t_g^+\to 0^-\right)=\mathbf{P}\mathbf{T}\left(t_g^+\to 0^+\right)\mathbf{P} \tag{3.27}$$

Where matrix $\overline{\mathbf{T}}$ satisfy the relation

$$\mathbf{V}\left(t_g^+\right)=\overline{\mathbf{T}}\left(t_g^+\to 0^-\right)\overline{\mathbf{V}}\left(0^-\right) \tag{3.28}$$

The next step to be dealt with is the excitation problem. The line source embedded in the air separating layer can also be expressed in terms of the superposition of PPWG modes, each of which is viewed as the incident mode for the scattering analysis. The line source placed at the center with amplitude I_0 could be expressed below

$$I_0\delta\left(x-w/2\right)=\sum_n \bar{I}_n\sqrt{\frac{2}{w}}\sin\left(\frac{n\pi x}{w}\right) \tag{3.29}$$

Taking the scalar products on the both sides of equalities (3.29) with the mode functions of the PPWG, we can determine the amplitude of each PPWG modes, as given by

$$\sum_n \bar{I}_n = I_0\sqrt{\frac{2}{w}}\sum_n \sin\left(\frac{n\pi}{2}\right) \tag{3.30}$$

The modal voltage waves at the position of line source relate to the excitation current amplitude and the input impedance of each PPWG mode looking upward and downward from the position of excitation; in the matrix form, they are given by

$$\overline{\mathbf{V}}\left(-d_1+d_2\right)=\left(\mathbf{Y}_{up}+\mathbf{Y}_{dn}\right)^{-1}\bar{\mathbf{I}} \tag{3.31}$$

where $\bar{\mathbf{I}}$ is the column vector with $\bar{I}_n$ as its elements at n-th entries.

Furthermore, the transmitted voltage (and current) waves of each waveguide mode from the position of excitation source to the outmost surface of the dielectric grating is determined by cascading the input-output relation derived previously. After taking the superposition for these transmitted voltage and current waves contributed by respective incident waveguide mode, the overall electric and magnetic fields distribution on the outmost surface of the antenna are obtained. Since this structure has only one open end, the backward and sideward radiations shall be negligible. The radiation far-field in the forward direction is determined using the two-dimensional Fourier transform of the aperture field on the outer surface of the dielectric grating. The equivalent- electric and magnetic currents on the outer surface are given as follows.

$$M_x(x) = -\sum_{n=1}^{\infty} \bar{V}_n(t_g^+)\phi_n(x) \qquad (3.32)$$

$$J_y(x) = \sum_{n=1}^{\infty} \bar{I}_n(t_g^+)\phi_n(x) \qquad (3.33)$$

Where *V*'s and *I*'s in (3.32) and (3.33) represent the voltage and current waves of each PPWG mode on the outmost surface. Notice that, in this research, we assumed that the electromagnetic fields have no variation along the *y* direction. Therefore, in the far-field radiation calculation, the equivalent sources were supposed to be uniform along the length of the radiating aperture, while the electric and magnetic fields are assumed to be vanished outside the radiation aperture.

3.3. NUMERICAL RESULTS

3.3.1 Effect of the relative dielectric constant on the radiation pattern

In figure 15, we fixed the thickness of the dielectric grating and changed the relative constant of dielectric rods from 2 to 6 to see the variation on the radiation pattern. As the relative dielectric constant increases, we observe that the radiation intensity in the two main lobe direction gradually increases. This phenomenon can be explained by the electric field distribution on the output surface of the grating. As shown in figure 16, the electric field magnitude increases, partially, in the dielectric grating region (x position from -4 to 4) while the relative dielectric constant increases. Thus the radiation intensity increases accordingly. As shown in figure 15, the difference between radiation pattern and target pattern is within 1 dB while the relative dielectric constant of dielectric grating varies from 3.5 to 4.5. It means that this antenna has the tolerance of 25% variation in the relative constant of dielectric rods.

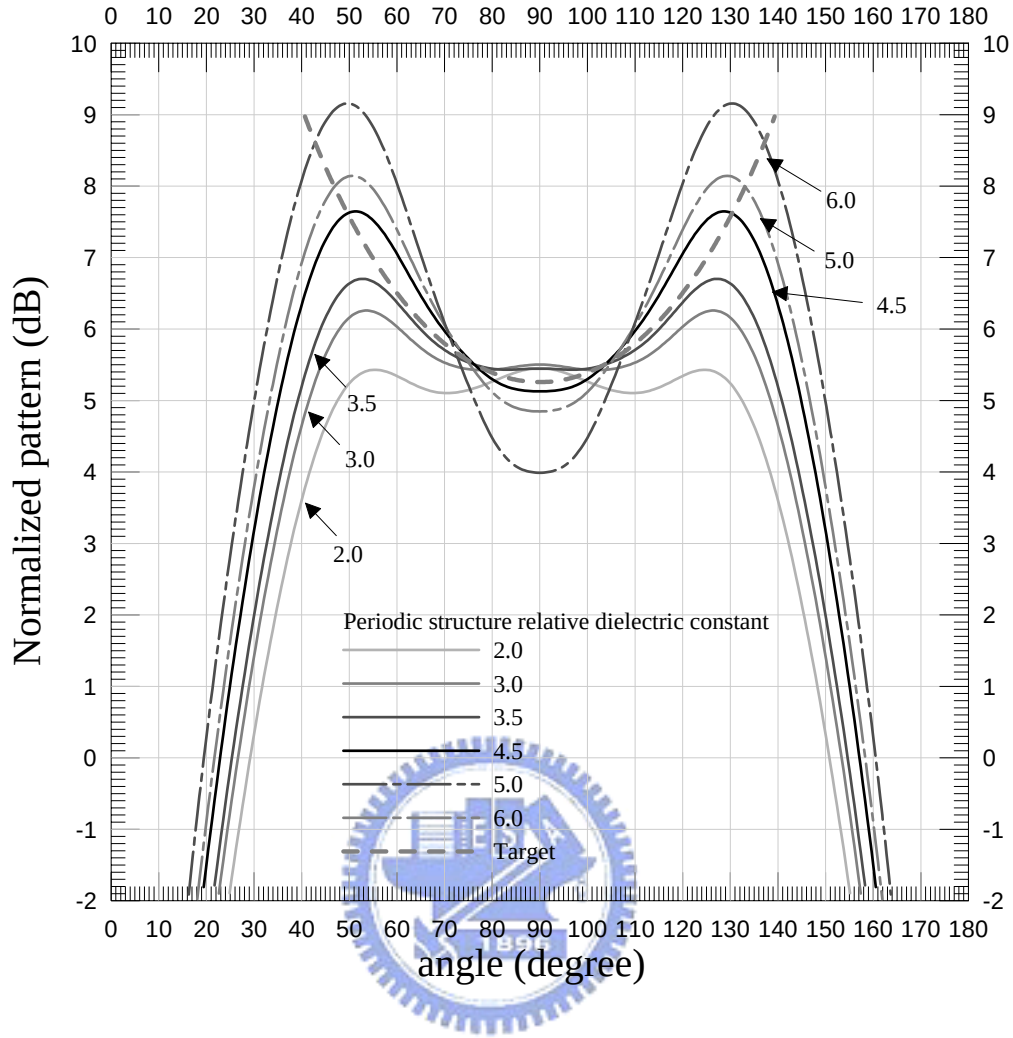

Figure 15: Radiation pattern for different dielectric constant at 5.4GHz (a=0.5 *cm*, b=1.0 *cm*, d_a=5 *cm*, t_g=0.2 *cm*, d_1=1.05 *cm*, d_2=0.68 *cm*)

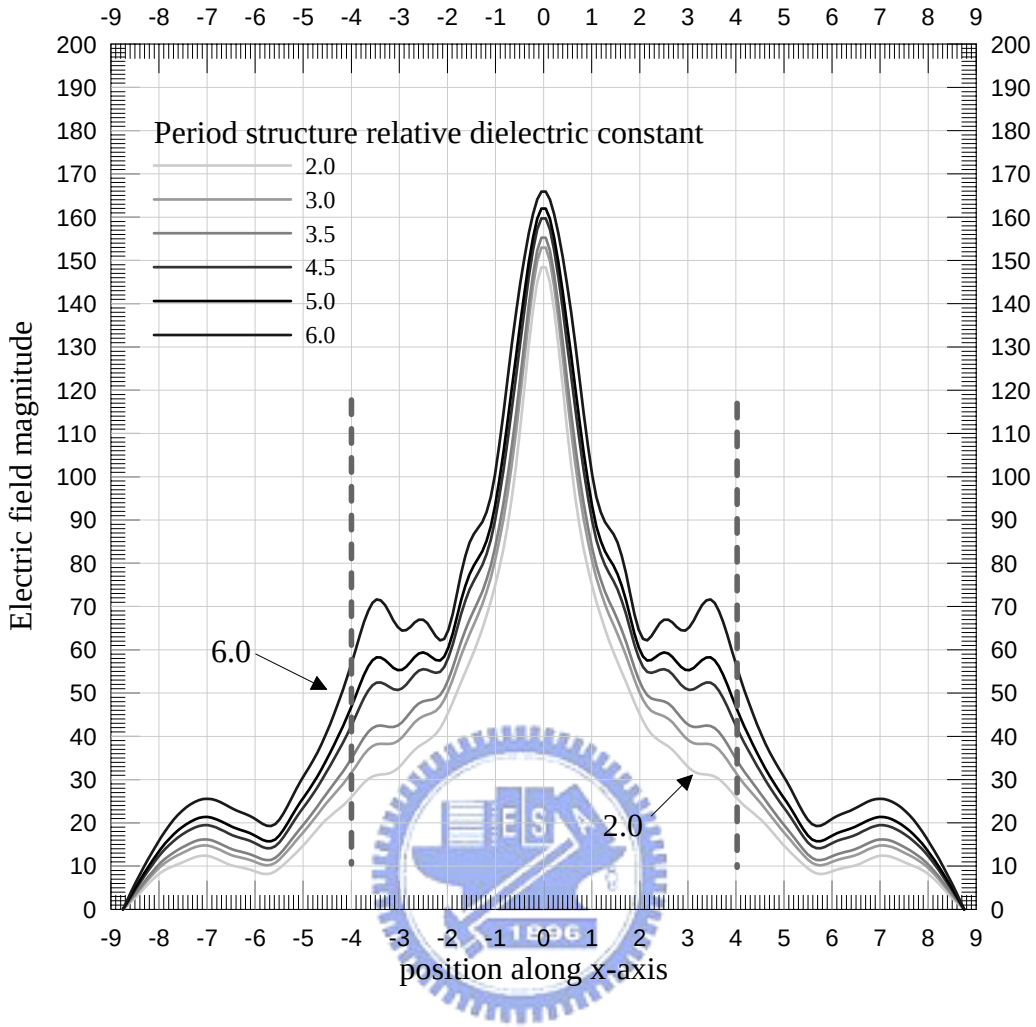

Figure 16: Electric field magnitude on the antenna aperture for different relative dielectric constant of dielectric rods at 5.4GHz (b=1.0 *cm*, d_a=5 *cm*, t_g=0.2 *cm*, d_1=1.05 *cm*, d_2=0.68 *cm*)

3.3.2 Effect of the aspect ratio of the grating layer on the radiation pattern

In Figure 17, we fixed the period of dielectric array (*b*) and changed the aspect ratio (*a/b*) from 0.02 to 0.8. For the small aspect ratio, the radiation pattern is dominated by the radiation intensity of space wave directly radiated by line source. As the aspect ratio increases: however, we observe that the radiation intensity of two radiation peaks gradually increases while the radiation intensity in the forward direction varies slightly. We may conjecture that the leaky wave phenomenon gradually become significant as the aspect ratio increases. Besides, the increase in the radiation intensity of the two radiation peaks may be explained by the increase of electric field magnitude in the output of dielectric grating region as shown in figure 18. Moreover, the aspect ratio of dielectric grating is an important parameter to adjust the intensity in the angular spectrum for obtaining the desired pattern.

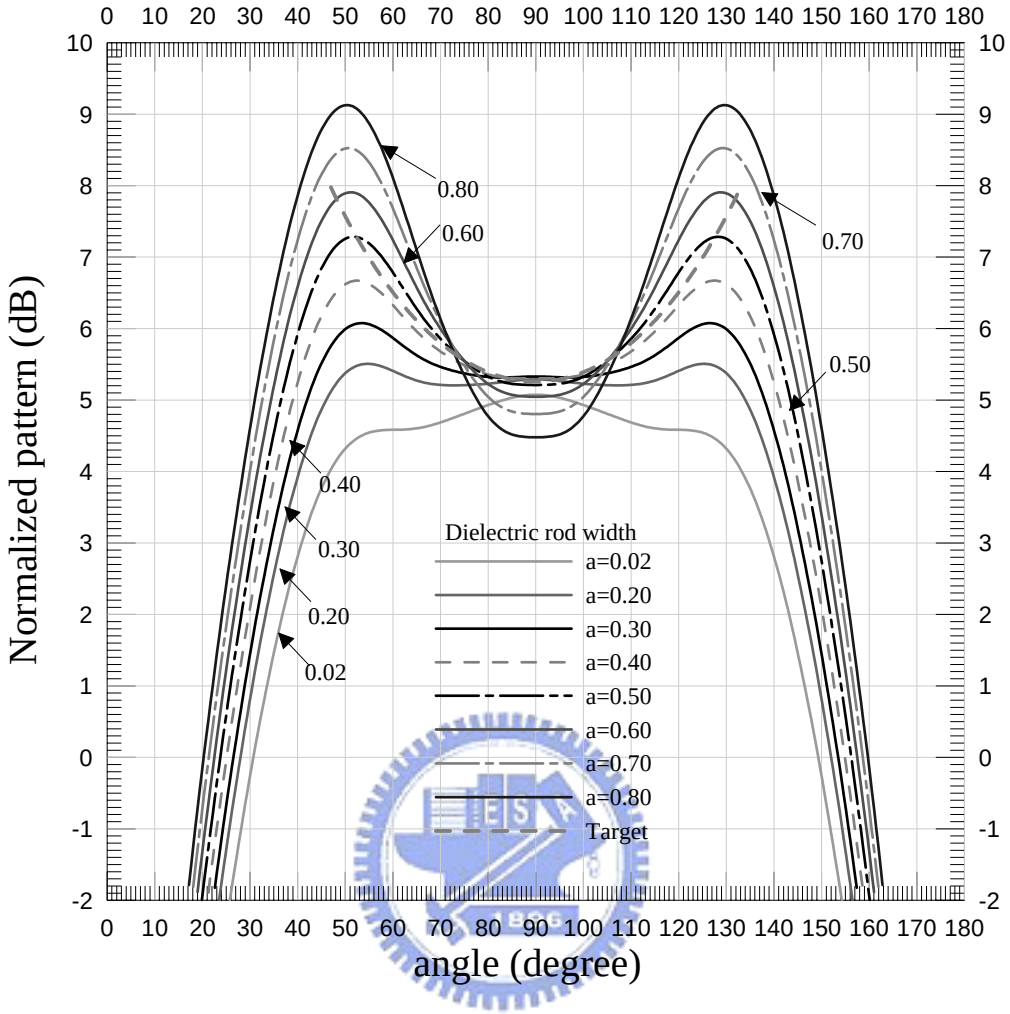

Figure 17: Radiation pattern for different aspect ratio at 5.4GHz (b=1.0 *cm*, d_a=5 *cm*, t_g=0.2 *cm*, d_1=1.05 *cm*, d_2=0.68 *cm*)

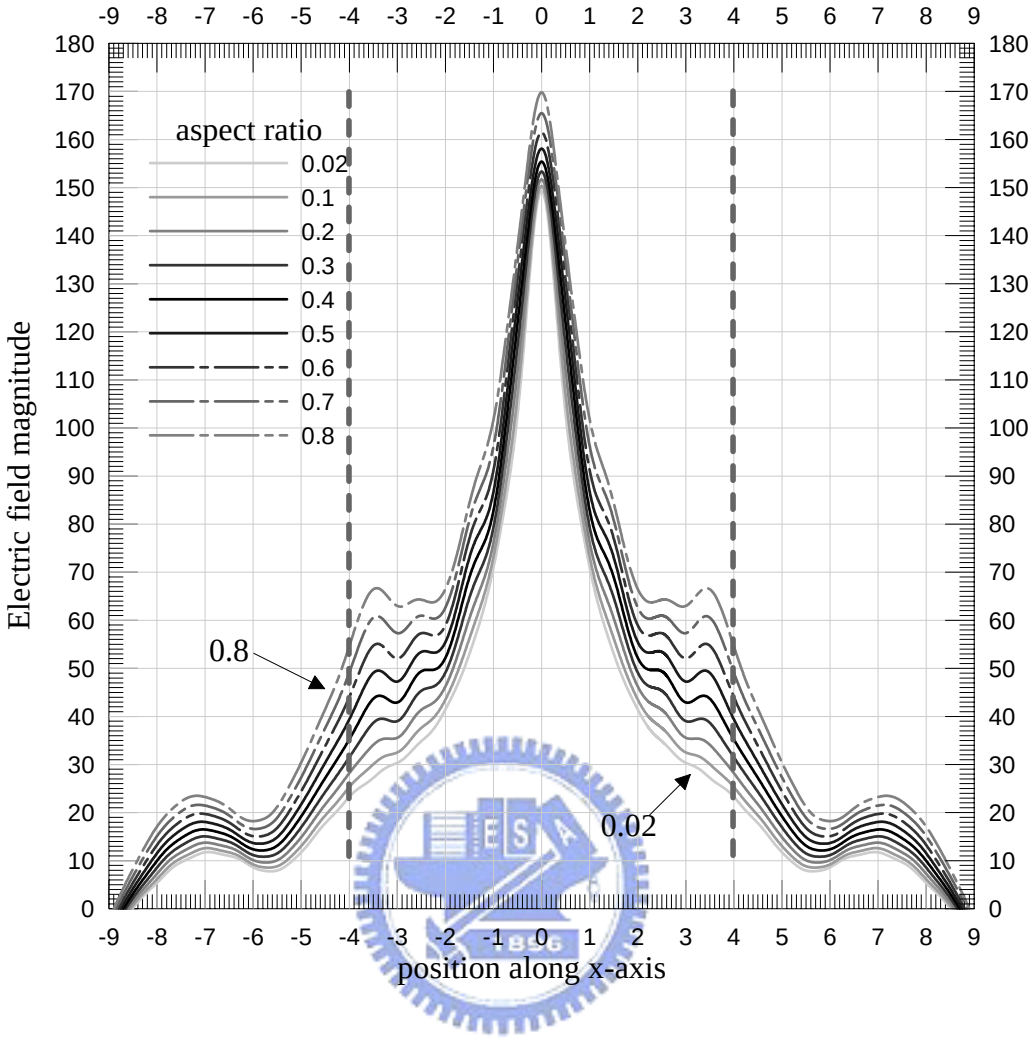

Figure 18: Electric field magnitude on the antenna aperture for different aspect ratio at 5.4GHz (b=1.0 *cm*, d_a=5 *cm*, t_g=0.2 *cm*, d_1=1.05 *cm*, d_2=0.68

3.3.3 Effect of the dielectric grating thickness on the radiation pattern

In Figure 19, we changed the thickness of the dielectric grating to see the variation on the radiation pattern. In this example, the dielectric substrate with the relative dielectric constant ε_r=4.2, and its thickness was varied from 0.10 to 0.40 (0.018 λ to 0.072 λ). We observe that the radiation intensity of two radiation peaks increases as the grating thickness increases. This phenomenon may be resulted from increasing in the electric field intensity on the output surface of dielectric grating layer as shown in figure 19. Evidently, the thickness of the grating is another important parameter for tuning the radiation pattern while it does not significantly affect the radiation angle.

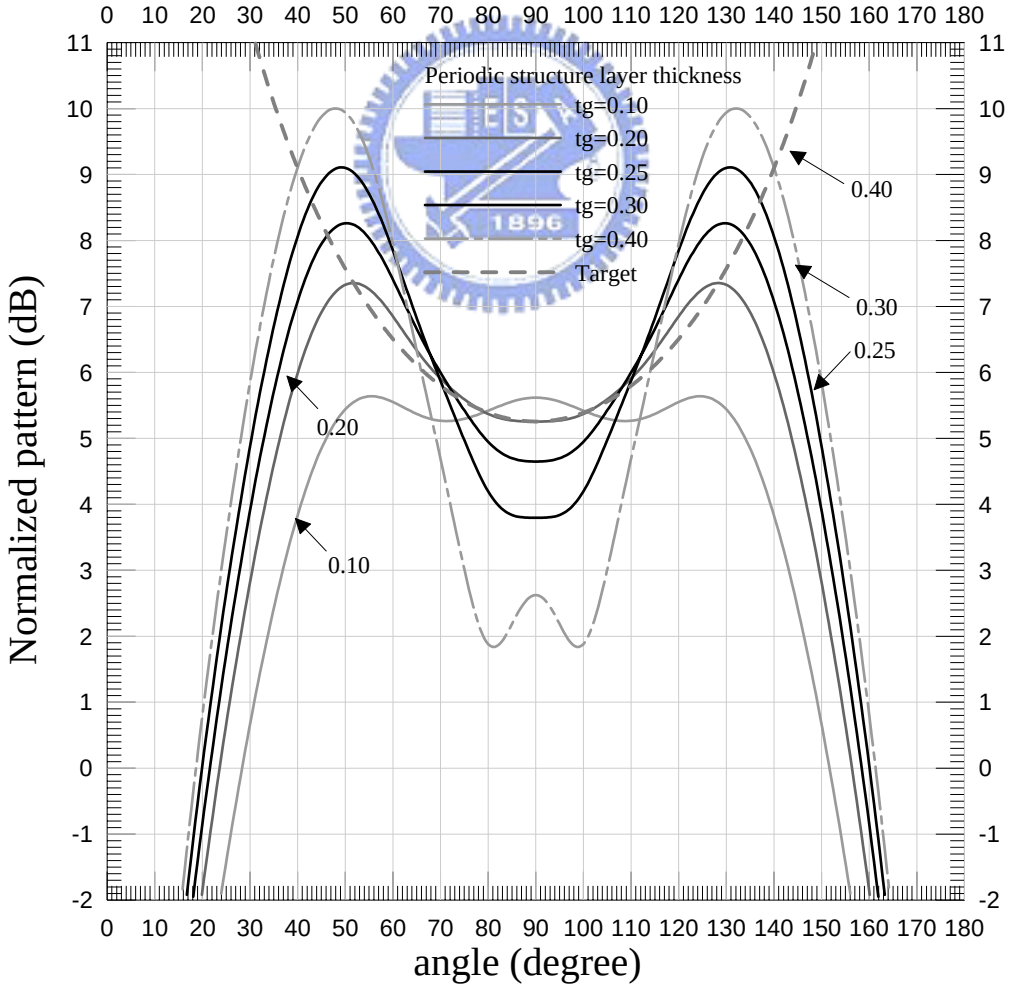

Figure 19: Radiation pattern for different dielectric grating layer thickness at 5.4GHz (*a*=0.5 *cm*, *b*=1.0 *cm*, d_a=5 *cm*, d_1=1.05 *cm*, d_2=0.68 *cm*)

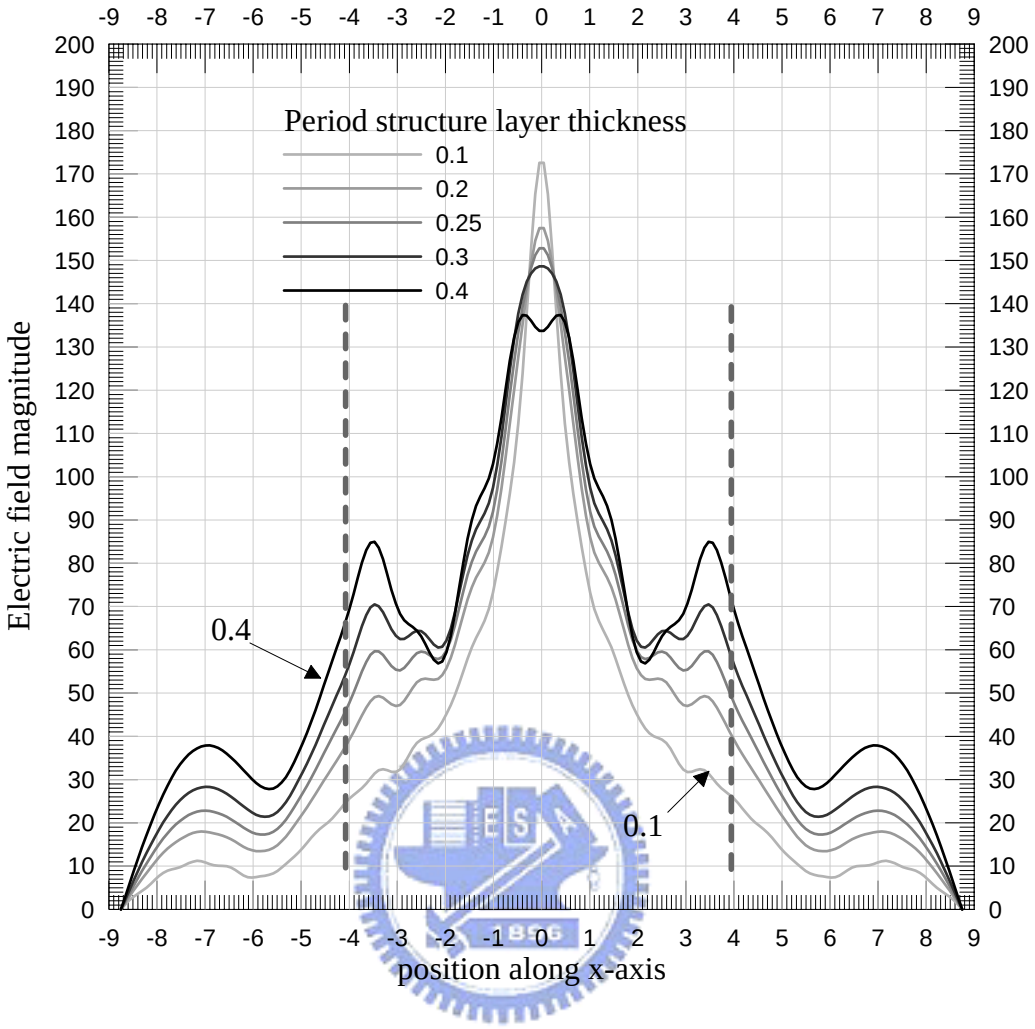

Figure 20: Electric field magnitude on the antenna aperture for different dielectric grating layer thickness at 5.4GHz (b=1.0 *cm*, d_a=5 *cm*, t_g=0.2 *cm*, d_1=1.05 *cm*, d_2=0.68 *cm*)

3.3.4 Effect of the line source position on the radiation pattern

In figure 21, we changed the position of the line source along the *z* direction to observe the variation on the far-field radiation pattern. From the previous examples, we know that the function of line source is to excite the waveguide mode propagating along the $\pm x$ direction. The propagating waveguide mode leaks its power into the surrounding medium. Since the offset of the position of line source only affect the strength of excited waveguide mode, the leaky wave angles (two radiation peaks) shall be unchanged. On the other hand, the radiation intensity in the forward direction (around 90 degree) changes since it is mainly contributed by the space wave radiation directly from the line source. Thus, we may observe that the field strength is decreasing as the line source is moving toward the metal plate. It may be explained by the image theory; that is, the image line source is directed opposite to that of the line source, reducing the strength in the far field. However, according to the curves shown in this figure, the position of line source can provide as a degree of flexibility in turning the radiation intensity while the beam shape remain unchanged.

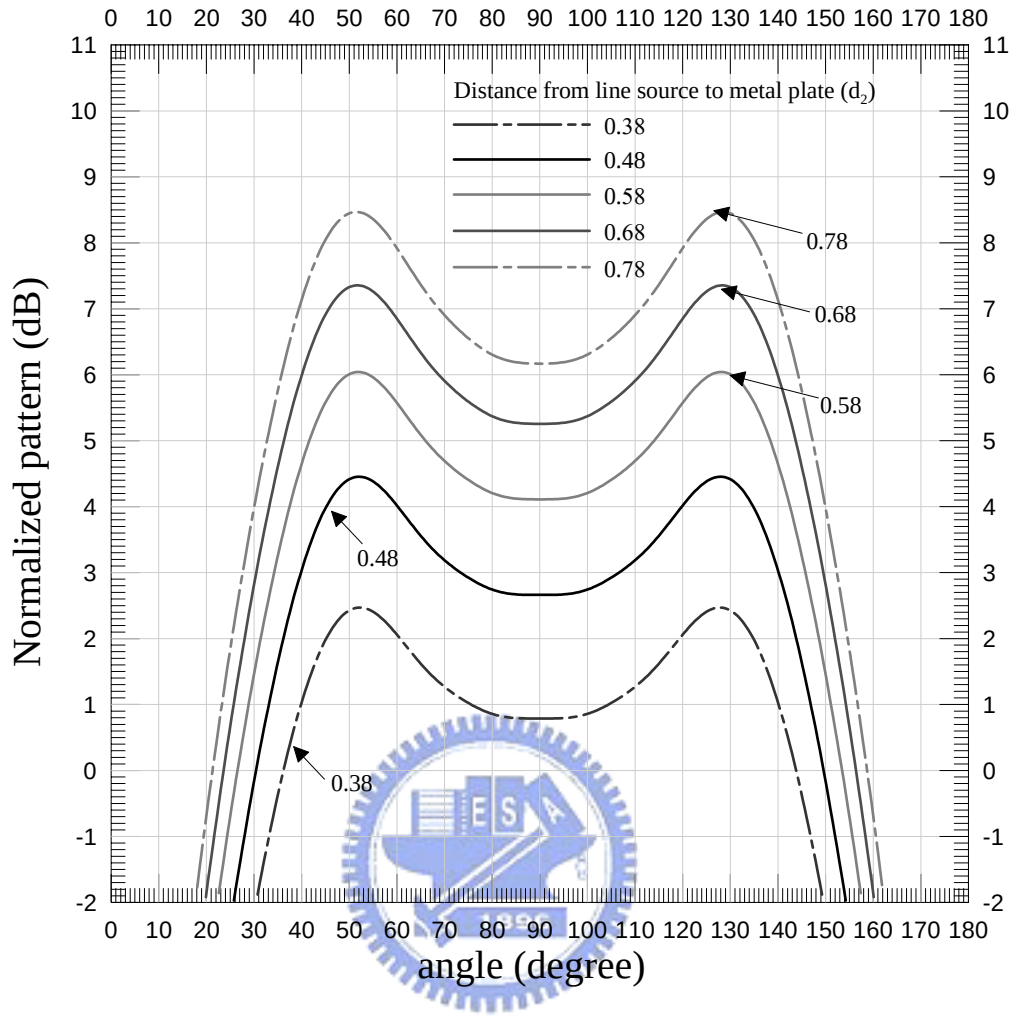

Figure 21: Radiation pattern for different distances from line source to metal ground plane at 5.4GHz (a=0.5 *cm*, b=1.0 *cm*, d_a=5 *cm*, t_g=0.2 *cm*, d_1=1.05 *cm*)

3.3.5 Frequency range of operation

In the pervious example, some parameters affecting the radiation pattern have been investigated. These results show that this antenna has considerable tolerance in the structure parameters while maintaining the desire pattern. In this example, we scanned the frequency from 4.8GHz to 6GHz to observe the variation on the radiation pattern. Then the bandwidth for obtaining the $\sec^2\theta$ radiation pattern could be realized from this example. From figure 22, we observed that the max deviation from the target pattern (angle from -40^o to 40^o) is within 1.25 dB for the frequencies ranging from 5.19GHz to 5.7GHz. Besides, the deviation is a positive value in the higher frequency range above 5.4GHz and a negative value in the lower frequency range. The radiated power deviation from the target pattern is within 1.25 dB in this frequency range, and the operation bandwidth is 9.37% around 5.445GHz. It is noted that the operation bandwidth is evaluated by the radiation pattern instead of the commonly used impedance bandwidth.

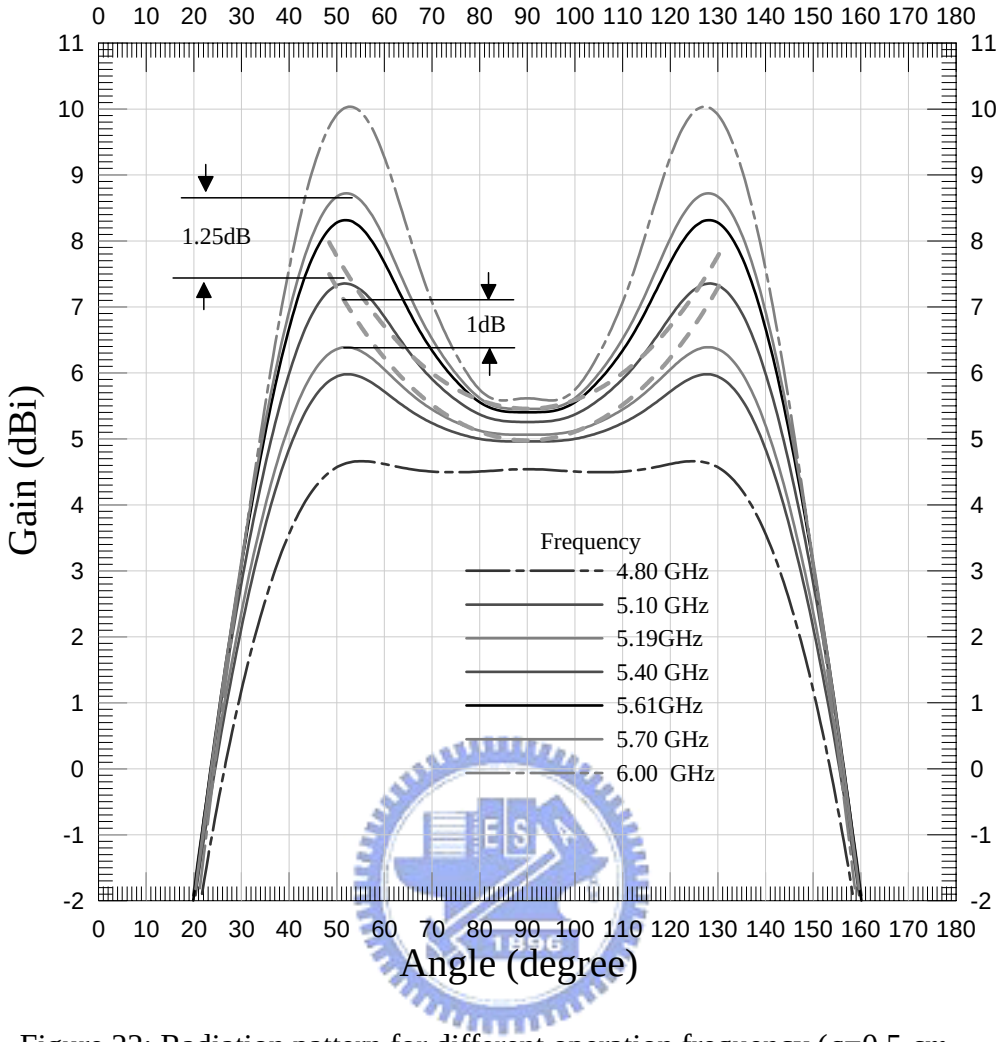

Figure 22: Radiation pattern for different operation frequency (a=0.5 *cm*, b=1.0 *cm*, d_a=5 *cm*, t_g=0.2 *cm*, d_1=1.05 *cm*, d_2=0.68 *cm*)

CHAPTER 4

Concluding Remarks

In this thesis, the prototype of a linear-polarized planar antenna radiating a rectangular footprint of uniform converge was presented. Combining the forward-, backward-leaky-wave and space wave radiation characteristics, the highly shaped-beam ($\sec^2$) pattern in the azimuthal plane was achieved. We have fabricated the antenna and measured its radiation characteristics. The bandwidth for maintaining a $\sec^2$ pattern (covering 80 degree) in the azimuthal plane is around 500 MHz. The rigorous mode-matching method incorporating the equivalent principle was employed to compute the far-field radiation pattern. The good agreement between the numerical and measured results was obtained. Furthermore, we have carried out the sensitivity analyses for the radiation pattern with respect to the changing in structure parameters and permittivity of the dielectric slab. Although the present antenna can not have the radiation characteristics of circular footprint coverage and circular polarization, it provides an alternative idea in synthesizing the highly shaped-beam pattern using leaky-wave characteristics of a periodic structure. The further work is to generate leaky waves along each radius direction on a circular aperture to produce circular footprint coverage.

REFERENCES

[1] A. A. Kishk, “Simple Primary Focus Feeds for Deep Reflector,” *Proc. IEE*, Vol. 136, pp 169-171. Apr. 1989.

[2] S. G. Hay, D. G. Bateman, T. S. Bird, F. R. Cooray, “Simple Ka-band Earth coverage antennas for LEO satellites,” *IEEE Antennas Propagation. Society Int. Symposium*, vol. 1, pp. 11-16, Jul. 1999.

[3] A. D. Olver, P. J. B. Clarricoats, A. A. Kishk and L. Shafai, *Microwave Horns and Feeds*, IEEE Press, New York, 1994.

[4] T. S. Bird, J. S. Kot, N. Nikolic, James, G. L. Barker, S.J., “Millimetre-wave antenna and propagation studies for indoor wireless LANs,” *Antennas and Propagation Society International Symposium*, vol. 1, pp. 336 - 339, Jun. 1994.

[5] P. F. M. Smulders, S. Khusial, M. H. A. J. Herben, “A shaped reflector antenna for 60-GHz indoor wireless LAN access points,” *IEEE Transactions on Vehicle Technology*, vol. 50, pp. 584 – 591, Mar. 2001.

[6] P. F. M. Smulders, M. H. A. J. Herben, “A shaped reflector antenna for 60-GHz radio access points,” *IEEE Transactions on Antennas Propagation*, vol. 49, pp. 1013 – 1015, Jul. 2001.

[7] A. Kumar, “Antennas for wireless indoor millimeter-waves applications,” *IEEE CCECE 2003*, vol. 3, pp. 1877 - 1880, May 2003.

[8] C. A. Balanis, *Antenna theory: analysis and design*, John Wiley & Sons, New York, 1997.

[9] H.-Y.D. Yang; D.R. Jackson, “Theory of line-source radiation from a metal-strip grating dielectric-slab structure,” *IEEE Transactions on Antennas and Propagation*, vol. 48, no. 4, pp.556-564, Apr. 2000.

[10] F. Capolino, D.R. Jackson, D.R. Wilton, “Fundamental properties of the field at the interface between air and a periodic artificial material excited by a line source,” *IEEE Transactions on Antennas and Propagation*, vol. 53, pp. 91 – 99 Jan. 2005.

[11] F. Capolino, D.R. Jackson, D.R. Wilton, “Mode excitation from sources in two-dimensional EBG waveguides using the array scanning method,” *IEEE Microwave and Wireless Components Letters*, Vol. 15, pp. 49 – 51, Feb. 2005.

[12] Giampiero Lovat, Paolo Burghignoli, Filippo Capolino, D. R. Jackson, and D. R. Wilton, “Analysis of Directive Radiation From a Line Source in a Metamaterial Slab With Low Permittivity,” *IEEE Transactions on Antennas and Propagation*, vol. 54, pp. 1017 – 1030, May 2006.

[13] T. Zhao, D. R. Jackson, J. T. Williams, H-Y D. Yang, A. A. Oliner, “2-D Periodic Leaky-Wave Antennas- Part I: Metal Patch Design,” *IEEE Transactions on Antennas and Propagation*, vol. 53, pp.3505 – 3514, Nov. 2005.

[14] Giampiero Lovat, Paolo Burghignoli, and D. R. Jackson, “Fundamental properties and optimization of broadside radiation from uniform leaky-wave antennas,” *IEEE Transactions on Antennas and Propagation*, vol. 54, pp. 1442 – 1452, May 2006

[15] J. Vazquaz, M. Shelley, P. De Maagt, “Parallel Plate photonic bandgap and periodic medium waveguides,” IEE Eleventh International conference on Antennas and Propagation ICAP2001, Manchester, United Kingdom, 17-20, April, 2001, pp 315-318

[16] D.R. Jackson, A.A. Oliner, A. Ip, “Leaky-wave propagation and radiation for a narrow-beam multiple-layer dielectric structure,” *IEEE Transactions on Antennas and Propagation*, Vol. 41, pp. 344 – 348, March 1993

[17] L. Leger, T. Monediere, B. Jecko, “Enhancement of gain and radiation bandwidth for a planar 1-D EBG Antenna,” *IEEE Microwave and wireless components letter*, vol. 15, no. 9, pp.573-575, Sep. 2005.

[18] A.R. Weily, L. Horvath, K.P. Esselle, B.C. Sanders, T.S. Bird, “A planar resonator antenna based on a woodpile EBG material,” *IEEE Transactions on Antennas and Propagation*, vol. 53, pp. 216 – 223, Jan. 2005.

APPENDIX I

Input-Output relation for a metal grating: Mode-matching

After collecting the modal- voltage and current in respective PPWGs, we could rewrite the equation (8-10) in terms of matrix-vector form given below.

$$\underline{V}(t_m^+) = \mathrm{R}^{(i)}\overline{\underline{V}}^{(i)}(t_m^-) \qquad \text{(A1.1)}$$

$$\overline{\underline{V}}^{(i)}(t_m^-) = \overline{\mathbf{R}}^{(i)}\underline{V}(t_m^+) \qquad \text{(A1.2)}$$

$$\overline{\underline{I}}^{(i)}(t_m^-) = \overline{\mathbf{R}}^{(i)}\underline{I}(t_m^+) \qquad \text{(A1.3)}$$

where the parameter *i* denotes the index number of the *i-th* aperture in the metal grating and the parameter *N* is the number of apertures. Parameter $\mathbf{R}^{(i)}$ is a coupling matrix, representing the electromagnetic field coupling between the oversized parallel-plate waveguide and the *i-th* sub-parallel-plate waveguide, with its *mn*th element given by

$$r_{mn}^{(i)} = \left\langle \phi_m(x) \middle| \overline{\phi}_n^{(i)}(x) \right\rangle \qquad \text{(A1.4)}$$

In addition, $\overline{\mathbf{R}}^{(i)}$ represents the transpose of matrix $\mathbf{R}^{(i)}$.

Having the relationship between the voltage and current waves in uniform dielectric layer and metal grating at the junction discontinuities, we could then develop the input-output relation of a metal grating layer, including the input impedance matrix and the voltage transfer matrix. Firstly, if the output admittance matrix of the metal grating layer is given by

$$\underline{I}(t_m^+) = \mathbf{Y}_l\underline{V}(t_m^+) \qquad \text{(A1.5)}$$

where t_m^+ represents the output surface position of the metal grating, in the oversized waveguide region. Substituting (A1.5) into equations (A1.1), (A1.2) and (A1.3), we could obtain the output admittance matrix at $z = t_m^-$, which is given below.

$$\underline{\bar{I}}(t_m^-) = \bar{\mathbf{Y}}_l \underline{\bar{V}}(t_m^-) \qquad \text{(A1.6)}$$

with $$\bar{\mathbf{Y}}_l = \bar{\mathbf{R}}\mathbf{Y}_l\mathbf{R}\,. \qquad \text{(A1.7)}$$

with $$\mathbf{R} = \begin{pmatrix}\mathbf{R_1} & \mathbf{R_2} & .... & \mathbf{R_{N-1}} & \mathbf{R_N}\end{pmatrix} \qquad \text{(A1.8)}$$

Where the super-matrix $\mathbf{R}$ contains each of the partition matrix $\mathbf{R}^{(i)}$. The super-vectors $\underline{\bar{V}}$ and $\underline{\bar{I}}$ were obtained by collecting each $\underline{\bar{V}}^{(i)}$ and $\underline{\bar{I}}^{(i)}$, respectively.

It can be shown, through a rather lengthy and involved derivation, we could obtain the input impedance matrix at $z = 0^+$, which is defined in the metal grating layer, given as

$$\bar{\mathbf{Z}}_{in}(0^+) = (\mathbf{I} + \bar{\mathbf{\Gamma}})(\mathbf{I} - \bar{\mathbf{\Gamma}})^{-1}\bar{\mathbf{Z}}_o \qquad \text{(A1.9)}$$

$$\bar{\mathbf{\Gamma}} = \exp(-j\bar{\mathbf{k}}_z t_m)\bar{\mathbf{\Gamma}}_l \exp(-j\bar{\mathbf{k}}_z t_m) \qquad \text{(A1.10)}$$

$$\bar{\mathbf{\Gamma}}_l = (\bar{\mathbf{Y}}_l + \bar{\mathbf{Y}}_o)(\bar{\mathbf{Y}}_o - \bar{\mathbf{Y}}_l)^{-1} \qquad \text{(A1.11)}$$

$$\bar{\mathbf{T}}(t_m^+ \to 0^+) = (\mathbf{I} + \bar{\mathbf{\Gamma}}_l)\exp(-j\bar{\mathbf{k}}_z t_m)(\mathbf{I} - \bar{\mathbf{\Gamma}})^{-1} \qquad \text{(A1.12)}$$

where $\bar{\mathbf{Z}}_o$ is a super-matrix containing each partition matrix $\bar{\mathbf{Z}}_o^{(i)}$ in each sub parallel-plate waveguide. The parameter $\bar{\mathbf{k}}_z$ is also a super diagonal matrix with each element representing the *z*-direction propagation constant of each mode in each sub parallel-plate waveguide. The matrix $\bar{\mathbf{T}}$ defines the relationship for the voltage waves at the input and output interfaces of the metal grating layer, which is given below

$$\underline{\bar{V}}(t_m^+) = \bar{\mathbf{T}}(t_m^+ \to 0^+)\underline{\bar{V}}(0^+) \qquad \text{(A1.13)}$$

Moreover, the input impedance, defined at the input interface in the oversized waveguide region, and the transfer matrix, defining the relationship between the output and input voltage waves through the metal grating layer, are give as follows.

$$\mathbf{Z}_{in}(0^-) = \mathbf{R}\mathbf{Z}_{in}(0^-)\overline{\mathbf{R}} \qquad \text{(A1.14)}$$

$$\mathbf{T}(t_m^+ \to 0^-) = \mathbf{R}\overline{\mathbf{T}}(t_m^+ \to 0^+)\overline{\mathbf{R}} \qquad \text{(A1.15)}$$

where the matrix **T** satisfy the relation

$$\underline{V}(t_m^+) = \mathbf{T}(t_m^+ \to 0^-)\underline{V}(0^-) \qquad \text{(A1.16)}$$

Radiation far-field calculation using equivalent principle

In addition to the input-output relationship of a metal-strip array layer, the input-output relation of a uniform dielectric layer filled in a parallel-plate waveguide could be obtained and be expressed in a similar form as shown in (A1.9). Since it is well-known and could be found in the literature, we neglect it in this section.

As mentioned earlier, this antenna is excited by a current source. The line source embedded in the air separating layer could be expressed in terms of the superposition of parallel-plate waveguide modes, each of which is viewed as the incident mode for the scattering analysis. The modal voltage waves at the position of line source could be written as

$$\underline{V}(z = -t_d - d_1 + d_2) = \left(\mathbf{Y}_{up} + \mathbf{Y}_{dn}\right)^{-1} I_o \underline{\phi}(x') \qquad \text{(A1.17)}$$

where $\mathbf{Y}_{\text{up}}$ and $\mathbf{Y}_{\text{dn}}$ are the input admittance matrices looking upward and downward from the position of line source, respectively. The parameter I_o is the amplitude of current source. The vector $\underline{\phi}$ is the vector containing each of the mode function evaluated at $x = x'$, $\{\phi_n(x')\}$.

APPENDIX II

Mode functions in the dielectric grating layer

The mode function and the propagation wave number of dielectric grating filled in PPWG is determined utilizing the transverse resonance technique. As shown in figure 15(a), the dielectric grating is a multilayer planar dielectric structure. The number of dielectric layer is *(p-1)/2* and *(p-1)/2+1* of air separator. We assume that the electromagnetic fields are invariant along the *y* the direction and propagate along the z direction. A transverse equivalent network for the dielectric grating in figure 15(a) is shown in figure 15(b). The propagation constant and characteristic impedance along x direction for n-th mode in p-th layer are given below.

$$\kappa_{pn} = \sqrt{k_0^2 \varepsilon_p - k_{zn}^2} = k_0 \sqrt{\varepsilon_p - \varepsilon_{effz}} \qquad \text{(A2.1)}$$

$$Z_{pn} = \begin{cases} \dfrac{\omega \mu_0}{\kappa_{pn}} & TE \bmod e \\ \dfrac{\kappa_{pn}}{\omega \varepsilon_0 \varepsilon_p} & TM \bmod e \end{cases} \qquad \text{(A2.2)}$$

Then we can obtain the input impedance looking upward and downward from the reference cut (dash line in figure 15(b)) by cascading of transmission line networks. The condition for resonance of the transmission line network can be written as

$$Z_{up} + Z_{dn} = 0 \qquad \text{(A2.3)}$$

For a given set of the grating structure parameters and a given operating frequency, we can solve the modal propagation constants k_{zn} from equation (A2.3). Substituting k_{zn} into (A2.2) and (A2.1), all the transmission line parameters in figure 15(b) are determined. Then the mode function ϕ_n for a given propagation constant k_{zn} can be determined. For TE mode, the mode function and the electric field component can be expressed as

$$E_{yn}(x,z) = -\phi_n(x)\exp(-jk_{zn}z) \tag{A2.4}$$

$$\phi_n(x) = \begin{cases} Z_{1,n}A_{1,n}\sin(\kappa_{1n}y + \theta_{1n}) \\ Z_{2,n}A_{2,n}\sin(\kappa_{2n}y + \theta_{2n}) \\ \vdots \\ Z_{(p-1),n}A_{(p-1),n}\sin(\kappa_{(p-1),n}y + \theta_{(p-1),n}) \\ Z_{p,n}A_{p,n}\sin(\kappa_{p,n}y + \theta_{p,n}) \end{cases} \tag{A2.5}$$

where n and p represent n-th propagation mode and p-th layer.

Based on the electromagnetic boundary conditions, the tangential electric and magnetic field must be continuous the discontinuities at the interface between two adjacent layer and vanish at PEC plane of the PPWG. We can determined the unknown parameters, $A_{p,n}$ and $\theta_{p,n}$, in each layer. Firstly, we set the value A_{1n} in the first layer to be 1, and the general solution of the amplitude and phase are given below

$$\theta_{p+1,n} = \tan^{-1}\left(\frac{Z_{p,n}}{Z_{p+1,n}}\tan(\kappa_{p,n} + \theta_{p,n})\right) - \kappa_{p+1,n}D_p \tag{A2.6}$$

$$A_{p+1,n} = A_{p,n}\frac{\cos(\kappa_{p,n}D_p + \theta_{p,n})}{\cos(\kappa_{p+1,n}D_p + \theta_{p+1,n})} \tag{A2.7}$$

$$D_p = \sum_{m=1}^{p} d_m \tag{A2.8}$$

Substituting the electric field (A2.4) into the Maxwell equations, we obtain a Sturm-Liouville differential equation (A2.9). Therefore the mode functions of a dielectric grating filled in PPWG are mutually orthogonal. With normalization, they can satisfy the orthogonal relation given below

$$\left[\frac{d}{dx}p(x)\frac{d}{dx} + q(x)\right]\phi_n(x) = k_{zn}^2 w(x)\phi_n(x) \tag{A2.9}$$

$$\langle \phi_m(y)|w(y)|\phi_n(y)\rangle = \delta_{mn} \tag{A2.10}$$

Where p, q and w are known functions for TE mode defined below

$$p(x) = w(x) = 1 \qquad \text{(A2.11)}$$

$$q(x) = k_0^2 \varepsilon_0 \varepsilon(x) \qquad \text{(A2.12)}$$

In figure 24, the first six modes of the dielectric grating used in the planar shaped beam antenna in chapter 3 are calculated. The dielectric grating filled in PPWG is composed of 8 dielectric layers and 9 air separators. The thickness and dielectric constant of dielectric layers are 0.5 and 4.2. The thickness of the outmost air separator is 5 and the thickness of others is 0.5. The effective dielectric constant of first six modes are 2.584, 2.335, 1.927, 1.384, 0.846 and 0.669 at the frequency k_0=0.18x2π. As shown in figure 16(a) to (d), the electric field concentrates in the dielectric grating region and decays in the outmost air separator for the effective dielectric constant grater than unity. The structure supports surface wave under such condition. For the effective dielectric constant is less than unity, the propagation constant of along x direction are real in all regions. Thus, we can observe that sinusoidal variation of field distribution in the PPWG.

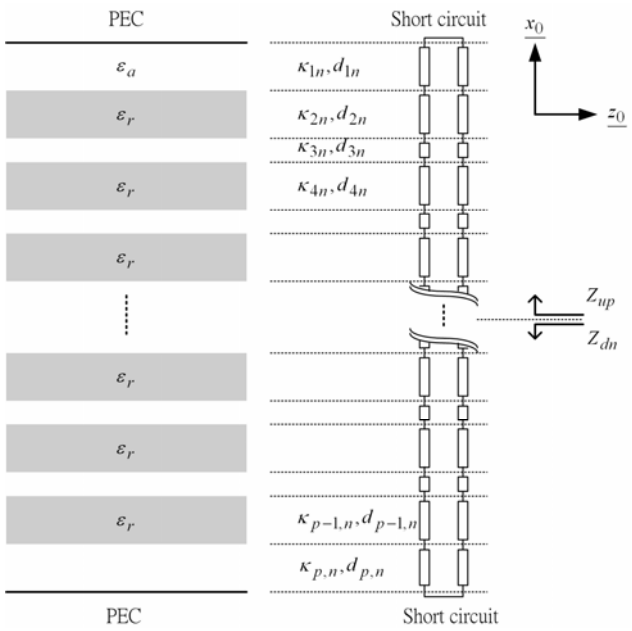

(a) (b)

Figure 23: Multiplayer planar structure and its equivalent network representation

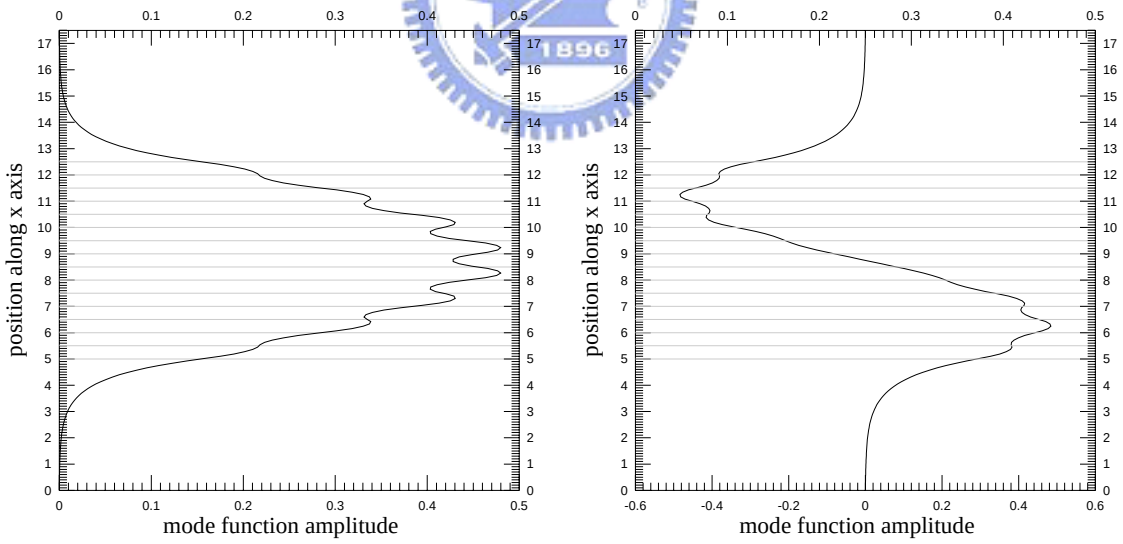

(a) (b)

Figure 24: Transverse field distribution of first six modes with effective dielectric constant; (a) 2.584, (b) 2.335.

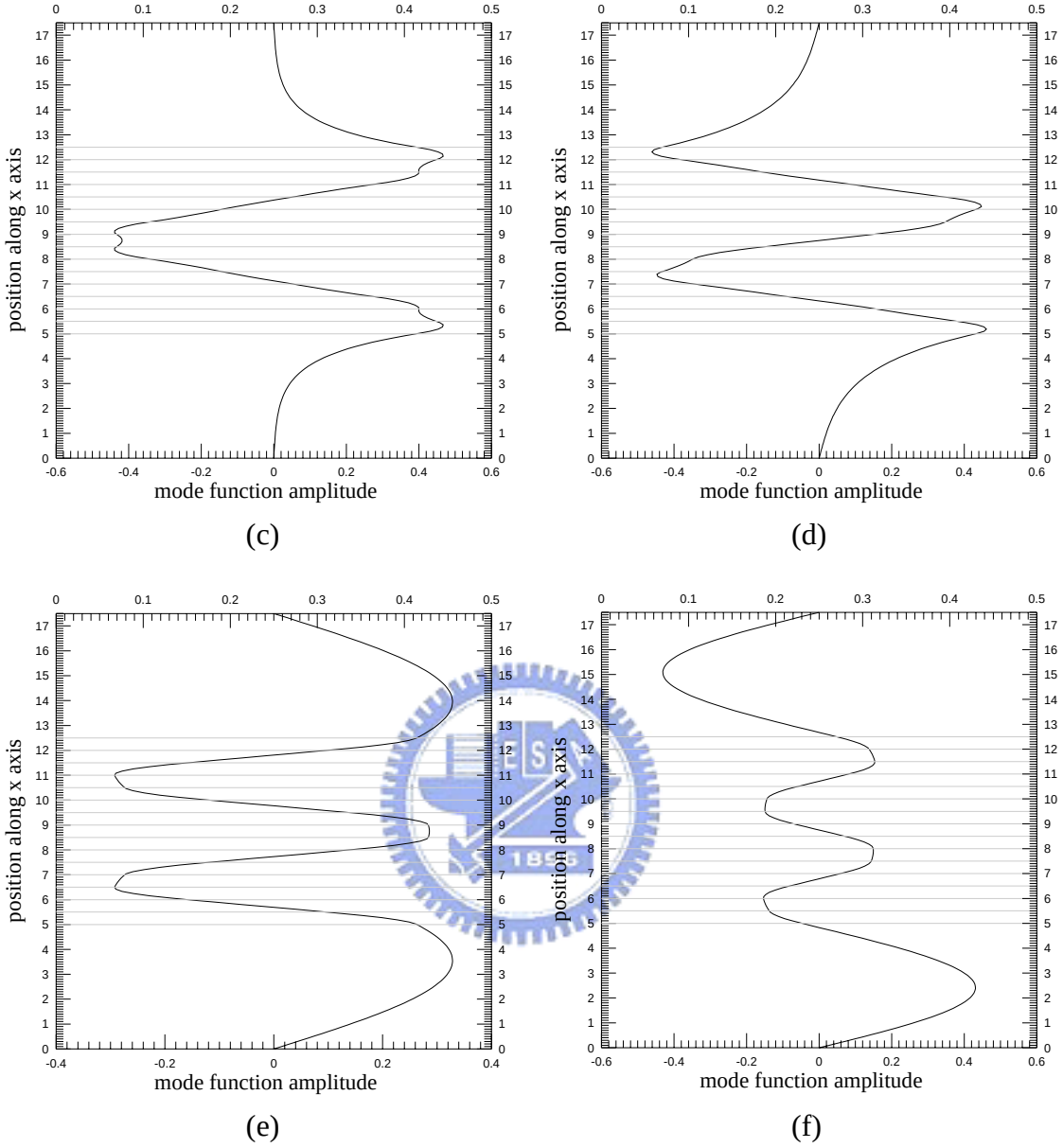

Figure 24: Transverse field distribution of first six modes with effective dielectric constant; (c) 1.927, (d) 1.384, (e) 0.846, (f) 0.669.

APPENDIX III

Far field calculation for aperture antenna

After obtaining the electromagnetic field excited by a line source on the antenna aperture, the equivalence principle is utilized to calculate the far field pattern of the aperture antenna. The equivalence principle replaces an aperture with equivalent currents J_s and M_s that produce radiation fields equivalent to those from the antenna. The radiation electric field arising from this electric and magnetic potential for z>0 is given below

$$\overline{E}_F = -j\omega\eta\left(F_\phi \underline{\theta} - F_\theta \underline{\phi}\right) \qquad \text{(A3.1)}$$

$$\overline{E}_A = -j\omega\left(A_\theta \underline{\theta} - A_\phi \underline{\phi}\right) \qquad \text{(A3.2)}$$

$$\overline{E} = \overline{E}_A + \overline{E}_F \qquad \text{(A3.3)}$$

The two dimensional Fourier transform of an aperture field is utilized to calculate radiation pattern, and we make the following definitions for the integral:

$$\overline{P} = \int\int_{S_a} \overline{E}_a e^{j\beta \bar{r}\cdot r'} ds' \qquad \text{(A3.4)}$$

$$\overline{Q} = \int\int_{S_a} \overline{H}_a e^{j\beta \bar{r}\cdot r'} ds' \qquad \text{(A3.5)}$$

The aperture surface is on the x-y plane, so $r' = x'\underline{x_0} + y'\underline{y_0}$. This with $\bar{r}$ in spherical coordinates in (A3.4) and (A3.5) yield

$$P_x = \int\int_{S_a} E_{ax} e^{j\beta\left(x'\sin\theta\cos\phi + y'\sin\theta\sin\phi\right)} dx'dy' \qquad \text{(A3.6)}$$

$$P_y = \int\int_{S_a} E_{ay} e^{j\beta\left(x'\sin\theta\cos\phi + y'\sin\theta\sin\phi\right)} dx'dy' \qquad \text{(A3.7)}$$

$$Q_x = \int\int_{S_a} H_{ax} e^{j\beta\left(x'\sin\theta\cos\phi + y'\sin\theta\sin\phi\right)} dx'dy' \qquad \text{(A3.8)}$$

$$Q_y = \int\int_{S_a} H_{ay} e^{j\beta\left(x'\sin\theta\cos\phi + y'\sin\theta\sin\phi\right)} dx'dy' \qquad \text{(A3.9)}$$

We can utilize above four equations to obtain the electric and magnetic potential given below

$$\overline{A} = \mu \frac{e^{-j\beta r}}{4\pi r}\left(-Q_y \hat{x} + Q_x \hat{y}\right) \qquad \text{(A3.10)}$$

$$\overline{F} = -\varepsilon \frac{e^{-j\beta r}}{4\pi r}\left(-P_y \hat{x} + P_x \hat{y}\right) \qquad \text{(A3.11)}$$

We can substitute the potential in (A3.10) add (A3.11) into (A3.3). Then, the final radiation components are given below

$$E_\theta = j\beta \frac{e^{-j\beta r}}{4\pi r}\left(P_x \cos\phi + P_y \sin\phi + \eta \cos\theta\left(Q_y \cos\phi - Q_x \sin\phi\right)\right) \qquad \text{(A3.12)}$$

$$E_\phi = j\beta \frac{e^{-j\beta r}}{4\pi r}\left(\cos\theta\left(P_y \cos\phi - P_x \sin\phi\right) - \eta\left(Q_y \sin\phi + Q_x \cos\phi\right)\right) \qquad \text{(A3.13)}$$